

# Highly Accurate Nyström Volume Integral Equation Method for the Maxwell equations for 3-D Scatters

Duan Chen<sup>a</sup> Wei Cai<sup>a</sup> Brian Zinser<sup>a</sup>

<sup>a</sup>*Department of Mathematics and Statistics, University of North Carolina at  
Charlotte, Charlotte, NC 28223, USA*

## **Suggested Running Head:**

Highly Accurate Nyström Volume Integral Equations for the  
Maxwell equations

## **Corresponding Author:**

Prof. Wei Cai

Department of Mathematics and Statistics,  
University of North Carolina at Charlotte,  
Charlotte, NC 28223-0001

Phone: 704-687-0628, Fax: 704-687-6415,

Email: wcai@uncc.edu

---

**Abstract**

In this paper, we develop highly accurate Nyström methods for the volume integral equation (VIE) of the Maxwell equation for 3-D scatters. The method is based on a formulation of the VIE equation where the Cauchy principal value of the dyadic Green's function can be computed accurately for a finite size exclusion volume with some explicit corrective integrals of removable singularities. Then, an effective interpolated quadrature formula for tensor product Gauss quadrature nodes in a cube is proposed to handle the hyper-singularity of integrals of the dyadic Green's function. The proposed high order Nyström VIE method is shown to have high accuracy and demonstrates  $p$ -convergence for computing the electromagnetic scattering of cubes in  $R^3$ .

*Key words:* Electromagnetic (EM) scattering, volume integral equation, Cauchy principal value, dyadic Green's function, Nyström methods.

---

## 1 Introduction

Electromagnetic (EM) wave scattering in the presence of (random) microstructure on material interfaces has a wide range of applications. For example, the interaction of light between the surface plasmon, a collective fluctuation of electron density under the background of the positive nucleus charges, on the metallic surfaces produces a so-called surface plasmon polariton (SPP) [1,11], which has important applications in solar cells [2], meta-materials, and super-resolution imaging devices [10,5]. Additionally, surface enhanced Raman scattering (SERS) [12] is also closely related to the excitation of surface plasmons on rough or nano-pattern surfaces by incident light and is an extremely useful tool in finger-printing the chemical components of a molecule, single molecule detector, detection of DNA studies, and bio-sensor, etc [6]. In all these applications, it is critical to have highly accurate and efficient numerical methods for computer simulations of the EM scattering in microstructures.

In this paper, we will present a high order Nyström volume integral equation (VIE) method for the time harmonic Maxwell equations using dyadic Green's functions  $\overline{\mathbf{G}}_{\mathbf{E}}(\mathbf{r}', \mathbf{r})$ . In most of the applications, the scatter is embedded into either a homogeneous or layered media and a Lippmann-Schwinger type of VIE, which is a well-conditioned second kind of Fredholm integral equation, can be derived for the regions occupied by the scatter while the

dyadic Green's function  $\overline{\mathbf{G}}_{\mathbf{E}}(\mathbf{r}', \mathbf{r})$  will ensure that the scattering field, expressed in terms of equivalent current sources inside the scatter, satisfies interface conditions along the layered interfaces as well as the Sommerfeld radiation conditions at  $\infty$ . In the VIE formulation, the electric field inside the scatter will use the Cauchy Principal Value (CPV or simply p.v.) associated with the dyadic Green's function as indicated in (19). Therefore, one of the most difficult issue is how to compute *accurately and efficiently* the CPV for the dyadic Green's function which has an  $O(\frac{1}{R^3})$  singularity, i.e.

$$\text{p.v.} \int_{\Omega} d\mathbf{r}' i\omega \Delta\epsilon(\mathbf{r}') \mathbf{E}(\mathbf{r}') \cdot \overline{\mathbf{G}}_{\mathbf{E}}(\mathbf{r}', \mathbf{r}) = \lim_{\delta \rightarrow 0} \int_{\Omega \setminus V_{\delta}} d\mathbf{r}' i\omega \Delta\epsilon(\mathbf{r}') \mathbf{E}(\mathbf{r}') \cdot \overline{\mathbf{G}}_{\mathbf{E}}(\mathbf{r}', \mathbf{r}), \quad (1)$$

where  $\Delta\epsilon(\mathbf{r}')$  describes the scatter dielectric constant deviating from the surrounding background material. As the CPV is defined through a limiting process of diminishing size  $\delta$  of the exclusion volume, in practical computation, a finite  $\delta$  has to be taken, namely, a small, finite and fixed  $\delta > 0$  for the exclusion  $V_{\delta}$  is selected, then the following approximation is taken

$$\text{p.v.} \int_{\Omega} d\mathbf{r}' i\omega \Delta\epsilon(\mathbf{r}') \mathbf{E}(\mathbf{r}') \cdot \overline{\mathbf{G}}_{\mathbf{E}}(\mathbf{r}', \mathbf{r}) \approx \int_{\Omega \setminus V_{\delta}} d\mathbf{r}' i\omega \Delta\epsilon(\mathbf{r}') \mathbf{E}(\mathbf{r}') \cdot \overline{\mathbf{G}}_{\mathbf{E}}(\mathbf{r}', \mathbf{r}). \quad (2)$$

Therefore, we are faced with two issues in the implementation of the VIE:

Firstly, what size of  $\delta$  should be taken? What is the effect of error by using a finite  $\delta$  in the calculation of the CPV? For any finite  $\delta$ , there will be a truncation error which we will call correction terms

$$\begin{aligned} \text{p.v.} \int_{\Omega} d\mathbf{r}' i\omega \Delta\epsilon(\mathbf{r}') \mathbf{E}(\mathbf{r}') \cdot \overline{\mathbf{G}}_{\mathbf{E}}(\mathbf{r}', \mathbf{r}) &= \int_{\Omega \setminus V_{\delta}} d\mathbf{r}' i\omega \Delta\epsilon(\mathbf{r}') \mathbf{E}(\mathbf{r}') \cdot \overline{\mathbf{G}}_{\mathbf{E}}(\mathbf{r}', \mathbf{r}) \\ &+ \text{correction terms.} \end{aligned} \quad (3)$$

The existence of these correction terms and their magnitude will limit the accuracy of the VIE solution if they are not explicitly included in the numerical solution process. The correction terms were derived by Fikioris [4] using the mixed potential formulation of the electric field. In this paper, we will re-derive the VIE similar to those in [4], however, in a more succinct manner and the final formula is more suitable for numerical implementations. Previous work on how to handle the singular integrals for VIE method include singularity subtraction [7], locally corrected Nyström scheme [9], direct integration of the singularity [14], etc.

Secondly, for the selected  $\delta$ , how to find an accurate integration quadrature formula to compute the resulting integration over the domain  $\Omega \setminus V_{\delta}$  with a highly singular integrand?

It is the objective of this paper to address these two issues and find easily implementable solutions. To address the first issue, we will derive the VIE

equation using vector and scale potentials such that the Cauchy principal value can be computed as in (3) with explicit expression for the correction terms. On the other hand, to address the second issue, we will construct special quadrature weights for the tensor product Gauss quadrature nodes in a reference element  $\Omega$  (taken to be a cube in this paper) by using an interpolation approach. In this approach, first a brute force computation of the integral, using Gauss quadrature in polar coordinate centered at the singularity, will be done to a given accuracy, albeit involving large number of values of the integrand. Then, realizing the integrand in the VIE matrix entries, except for the singular denominators involving  $R^k$ ,  $1 \leq k \leq 3$ , are smooth functions, which can be in fact accurately interpolated using values on the tensor product Gauss nodes inside the cubic domain  $\Omega$ . Then, the brute-force integration formula can be converted into a new integration weights for the tensor product Gauss nodes. The new integration formula can be tabulated for integrating general functions. Finally, the Nyström collocation method is used to discretize the VIE with a high order accuracy.

The rest of the paper is organized as follows: Section 2 presents the formulation of a VIE where the CPV can be computed with a finite exclusion volume accurately. Then, numerical algorithms, including the Nyström collocation method, efficient quadrature formula and numerical implementation are given in Section 3. Section 4 includes various numerical simulation tests such as the accuracy of Cauchy principal value computation,  $\delta$ -independence of matrix entries and  $p$ -refinement convergence for the VIE. The paper ends with a conclusion in Section 5.

## 2 Volume Integral equations for the Maxwell equations

### 2.1 VIE and Cauchy principal values

In this section, we will follow [3] to show briefly how the VIE for the Maxwell equations can be derived using a vector form second Green's identity for the following vector wave equations,

$$\mathcal{L}\mathbf{E}(\mathbf{r}) - \omega^2\epsilon(\mathbf{r})\mathbf{E}(\mathbf{r}) = -i\omega\mathbf{J}_e(\mathbf{r}), \quad \mathbf{r} \in \mathbb{R}^3 \setminus (\Sigma \cup \partial\Omega), \quad (4)$$

where  $\omega$  is the frequency,  $\mu$  is the permeability, and  $\Sigma$  consists of any possible interfaces of the background medium in case of a layered material,

$$\mathcal{L} = \nabla \times \frac{1}{\mu} \nabla \times,$$

and  $\mathbf{J}_e(\mathbf{r})$  is the far-field source (assumed to be away from the layered structure), which produces the incident waves impinging on the layered structure from the top, i.e.,

$$\mathbf{E}^{\text{inc}}(\mathbf{r}) = -i\omega\mu(\mathbf{r}) \int_{\mathbb{R}^3} \overline{\mathbf{G}}_E(\mathbf{r}, \mathbf{r}') \cdot \mathbf{J}_e(\mathbf{r}') d\mathbf{r}', \quad (5)$$

and  $\overline{\mathbf{G}}_E(\mathbf{r}, \mathbf{r}')$  is the dyadic Green's function for the layered media. A scatter  $\Omega$  is characterized by a different dielectric constant from the layered background dielectrics, i.e.,

$$\epsilon(\mathbf{r}) = \epsilon_L(\mathbf{r}) + \Delta\epsilon(\mathbf{r}), \quad (6)$$

where  $\Delta\epsilon(\mathbf{r}) = 0, \mathbf{r} \notin \Omega$ . Then, (4) can be rewritten as

$$\mathcal{L}\mathbf{E}(\mathbf{r}) - \omega^2\epsilon_L(\mathbf{r})\mathbf{E}(\mathbf{r}) = -i\omega\mathbf{J}(\mathbf{r}), \quad (7)$$

where

$$\mathbf{J}(\mathbf{r}) = \mathbf{J}_e(\mathbf{r}) + \mathbf{J}_{\text{eq}}(\mathbf{r}), \quad (8)$$

and the equivalent current source  $\mathbf{J}_{\text{eq}}(\mathbf{r})$  is defined to reflect the existence of the scatter  $\Omega$ :

$$\mathbf{J}_{\text{eq}}(\mathbf{r}) = i\omega\Delta\epsilon(\mathbf{r})\mathbf{E}(\mathbf{r}). \quad (9)$$

Let us consider any interior point inside the scatter, i.e.,  $\mathbf{r}' \in \Omega$  and a small volume  $V_\delta = V_\delta(\mathbf{r}') \subset \Omega$  centered at  $\mathbf{r}'$ . The dyadic Green's function  $\overline{\mathbf{G}}_E(\mathbf{r}, \mathbf{r}')$  is defined by

$$\mathcal{L}\overline{\mathbf{G}}_E(\mathbf{r}, \mathbf{r}') - \omega^2\epsilon_L(\mathbf{r})\overline{\mathbf{G}}_E(\mathbf{r}, \mathbf{r}') = \frac{1}{\mu(\mathbf{r})} \overline{\mathbf{I}}\delta(\mathbf{r} - \mathbf{r}'), \quad \mathbf{r} \in \mathbb{R}^3. \quad (10)$$

In the case of a homogeneous medium, we have

$$\overline{\mathbf{G}}_E(\mathbf{r}, \mathbf{r}') = \overline{\mathbf{G}}_E(\mathbf{r}', \mathbf{r}) = \left( \overline{\mathbf{I}} + \frac{1}{k^2} \nabla \nabla \right) g(\mathbf{r}, \mathbf{r}'), \quad (11)$$

where  $k^2 = \omega^2\epsilon_i\mu$ ,  $\epsilon_i = \epsilon_L(\mathbf{r})$ ,  $\mu$  is the permeability of the medium, and

$$g(\mathbf{r}, \mathbf{r}') = \frac{1}{4\pi} \frac{e^{-ikR}}{R}, \quad R = |\mathbf{r} - \mathbf{r}'|. \quad (12)$$

Next, on multiplying (7) by  $\overline{\mathbf{G}}_E(\mathbf{r}, \mathbf{r}')$  and (10) by  $\mathbf{E}(\mathbf{r})$  and forming the difference, and then integrating over the domain  $\mathbb{R}^3 \setminus V_\delta$ , after some manipula-

tion [3], we arrive at the following equation (after switching  $\mathbf{r}$  and  $\mathbf{r}'$ ):

$$\begin{aligned} & -i\omega\mu(\mathbf{r}) \int_{\mathbb{R}^3 \setminus V_\delta} d\mathbf{r}' \overline{\mathbf{G}}_E(\mathbf{r}, \mathbf{r}') \cdot \mathbf{J}(\mathbf{r}') - \mu(\mathbf{r}) \int_{S_\delta} ds' \left[ i\omega \overline{\mathbf{G}}_E(\mathbf{r}, \mathbf{r}') \cdot (\mathbf{n} \times \mathbf{H}(\mathbf{r}')) \right. \\ & \left. - \frac{1}{\mu(\mathbf{r}')} \nabla \times \overline{\mathbf{G}}_E(\mathbf{r}, \mathbf{r}') \cdot (\mathbf{n} \times \mathbf{E}(\mathbf{r}')) \right] = \mathbf{0}, \quad \mathbf{r} \in \Omega, \end{aligned} \quad (13)$$

where  $S_\delta = \partial V_\delta(\mathbf{r})$ ,  $\mathbf{n}$  is the normal of  $S_\delta$  pointing out of  $V_\delta(\mathbf{r})$ .

As  $\delta \rightarrow 0$ , the first integral will approach the Cauchy principal value of a singular integral, while the surface integrals will in fact depend on the geometric shape of the volume  $V_\delta$ .

In order to estimate the surface integrals, we have the following asymptotics for small  $kR \ll 1$ :

$$\overline{\mathbf{G}}_E(\mathbf{r}, \mathbf{r}') = \frac{1}{4\pi k^2 R^3} (\mathbf{I} - 3\mathbf{u} \otimes \mathbf{u}) + O\left(\frac{1}{R^2}\right), \quad (14)$$

$$\nabla' \times \overline{\mathbf{G}}_E(\mathbf{r}, \mathbf{r}') = \frac{1}{4\pi R^2} \mathbf{u} \times \mathbf{I} + O\left(\frac{1}{R}\right), \quad (15)$$

where  $\mathbf{u} = (\mathbf{r}' - \mathbf{r})/R$ , which implies that:

$$\lim_{\delta \rightarrow 0} \int_{S_\delta} ds' \mathbf{n} \times \mathbf{E}(\mathbf{r}') \cdot \nabla \times \overline{\mathbf{G}}_E(\mathbf{r}', \mathbf{r}) = -[\mathbf{I} - \mathbf{L}_{V_\delta}] \cdot \mathbf{E}(\mathbf{r}), \quad (16)$$

$$\lim_{\delta \rightarrow 0} \int_{S_\delta} ds' \mathbf{n} \times \mathbf{H}(\mathbf{r}') \cdot \overline{\mathbf{G}}_E(\mathbf{r}', \mathbf{r}) = -\frac{1}{k^2} \mathbf{L}_{V_\delta} \cdot \nabla \times \mathbf{H}(\mathbf{r}), \quad (17)$$

and the  $\mathbf{L}$ -dyadics for  $V_\delta$  of various geometric shapes are given as follows [16]:

$$\mathbf{L}_{V_\delta} = \frac{1}{3} \mathbf{I} \quad (18)$$

for a sphere.

Substituting (16) and (17) into (13), after some manipulation and also using Ampère's law, we have the VIE for the electric field for  $\mathbf{r} \in \Omega$ :

$$\mathbf{C} \cdot \mathbf{E}(\mathbf{r}) = \mathbf{E}^{\text{inc}}(\mathbf{r}) - i\omega\mu(\mathbf{r}) \text{ p.v. } \int_{\Omega} d\mathbf{r}' i\omega\Delta\epsilon(\mathbf{r}') \mathbf{E}(\mathbf{r}') \cdot \overline{\mathbf{G}}_E(\mathbf{r}', \mathbf{r}), \quad (19)$$

where the coefficient matrix is given by

$$\mathbf{C} = \mathbf{I} + \mathbf{L}_{V_\delta} \cdot \Delta\epsilon(\mathbf{r}). \quad (20)$$

As mentioned in the introduction, in most numerical implementations of (19), the CPV integral is computed by selecting a finite  $\delta$  as in (2), therefore the numerical solution thus obtained does not satisfy the original VIE (19) and it will have an intrinsic error reflected in the correction terms indicated in (3).

## 2.2 Reformulation of the VIE and computing CPV with a finite $\delta$

In this section, we will derive a VIE of the E-field where the CPV in (20) can be computed with a finite exclusion volume together with some correction terms. Based on the Helmholtz decomposition, the electric field  $\mathbf{E}(\mathbf{r})$  can be expressed as follows [3],

$$\mathbf{E} = -i\omega\mathbf{A} - \nabla V,$$

according to the Lorentz gauge [13],

$$\nabla \cdot \mathbf{A} = -i\omega\epsilon\mu V, \quad (21)$$

so we have a vector potential representation for the electric field,

$$\mathbf{E} = -i\omega\mathbf{A} + \frac{1}{i\omega\epsilon\mu}\nabla(\nabla \cdot \mathbf{A}) = -i\omega\left[\bar{\mathbf{I}} + \frac{1}{k^2}\nabla\nabla\right]\mathbf{A}. \quad (22)$$

On the other hand, it can be shown that the potential  $\mathbf{A}$  satisfies the Helmholtz equation componentwise [3]

$$\nabla^2\mathbf{A} + k^2\mathbf{A} = -\mu\mathbf{J}. \quad (23)$$

Thus the solution  $\mathbf{A}$  of Eq. (23) can be rewritten as an integral representation:

$$\begin{aligned} \mathbf{A} &= \mu \int_{\mathbb{R}^3} d\mathbf{r}' \mathbf{J}(\mathbf{r}') g(\mathbf{r}, \mathbf{r}') \\ &= \mu \int_{\mathbb{R}^3 \setminus \Omega} \mathbf{J}_e(\mathbf{r}') g(\mathbf{r}, \mathbf{r}') d\mathbf{r}' + \mu \int_{\Omega} \mathbf{J}_{eq}(\mathbf{r}') g(\mathbf{r}, \mathbf{r}') d\mathbf{r}' \\ &= \mu \int_{\mathbb{R}^3 \setminus \Omega} \mathbf{J}_e(\mathbf{r}') g(\mathbf{r}, \mathbf{r}') d\mathbf{r}' + \mu \int_{\Omega} d\mathbf{r}' i\omega\Delta\epsilon(\mathbf{r}') \mathbf{E}(\mathbf{r}') g(\mathbf{r}, \mathbf{r}'), \end{aligned} \quad (24)$$

where the second equality on the right hand side of Eq. (24) is due to the assumption that  $\text{supp}(\mathbf{J}_e(\mathbf{r})) \cap \Omega = \emptyset$ .

For the first integral in Eq. (24), it is well-defined if  $\mathbf{r} \in \Omega$  and when we plug it into Eq. (22), it yields the incident wave  $\mathbf{E}^{\text{inc}}(\mathbf{r})$  according to relation (5). For the second integral over  $\Omega$ , we split it as follows

$$\mu \int_{\Omega} d\mathbf{r}' i\omega\Delta\epsilon(\mathbf{r}') \mathbf{E}(\mathbf{r}') g(\mathbf{r}, \mathbf{r}') = \mu \left( \int_{\Omega \setminus V_\delta} + \int_{V_\delta} \right) i\omega\Delta\epsilon(\mathbf{r}') \mathbf{E}(\mathbf{r}') g(\mathbf{r}, \mathbf{r}'),$$

and along with the first integral term in Eq. (24), it follows from Eq. (22) that

$$\begin{aligned}
\mathbf{E} &= \mathbf{E}^{\text{inc}}(\mathbf{r}) - i\omega \int_{\Omega \setminus V_\delta} i\omega \Delta\epsilon(\mathbf{r}') \mathbf{E}(\mathbf{r}') \left[ \bar{\mathbf{I}} + \frac{1}{k^2} \nabla \nabla \right] g(\mathbf{r}, \mathbf{r}') \\
&\quad - i\omega \left[ \bar{\mathbf{I}} + \frac{1}{k^2} \nabla \nabla \right] \int_{V_\delta} d\mathbf{r}' i\omega \Delta\epsilon(\mathbf{r}') \mathbf{E}(\mathbf{r}') g(\mathbf{r}, \mathbf{r}') \\
&= \mathbf{E}^{\text{inc}}(\mathbf{r}) - i\omega \int_{\Omega \setminus V_\delta} i\omega \Delta\epsilon(\mathbf{r}') \bar{\mathbf{G}}_{\mathbf{E}}(\mathbf{r}, \mathbf{r}') \cdot \mathbf{E}(\mathbf{r}') \\
&\quad - i\omega \left[ \bar{\mathbf{I}} + \frac{1}{k^2} \nabla \nabla \right] \int_{V_\delta} d\mathbf{r}' i\omega \Delta\epsilon(\mathbf{r}') \mathbf{E}(\mathbf{r}') g(\mathbf{r}, \mathbf{r}'). \tag{25}
\end{aligned}$$

Next, we isolate the singular part from  $g(\mathbf{r}, \mathbf{r}')$  as follows

$$g(\mathbf{r}, \mathbf{r}') = g_0(\mathbf{r}, \mathbf{r}') + \tilde{g}(\mathbf{r}, \mathbf{r}'), \tag{26}$$

where

$$g_0(\mathbf{r}, \mathbf{r}') = \frac{1}{4\pi|\mathbf{r} - \mathbf{r}'|}, \tag{27}$$

and use the fact that [8,16]

$$\nabla \nabla \int_{V_\delta} d\mathbf{r}' \frac{1}{4\pi|\mathbf{r} - \mathbf{r}'|} = - \int_{\partial V_\delta} ds' \frac{(\mathbf{r} - \mathbf{r}') \mathbf{u}_n(\mathbf{r}')}{4\pi|\mathbf{r} - \mathbf{r}'|^3} = -\mathbf{L}_{V_\delta}, \tag{28}$$

we can compute the following integral in the following manner

$$\begin{aligned}
&\nabla \nabla \int_{V_\delta} d\mathbf{r}' \Delta\epsilon(\mathbf{r}') \mathbf{E}(\mathbf{r}') g_0(\mathbf{r}, \mathbf{r}') \\
&= \nabla \nabla \int_{V_\delta} d\mathbf{r}' \frac{1}{4\pi|\mathbf{r} - \mathbf{r}'|} \Delta\epsilon(\mathbf{r}') \mathbf{E}(\mathbf{r}') + \int_{V_\delta} d\mathbf{r}' \nabla \nabla g_0(\mathbf{r}, \mathbf{r}') [\Delta\epsilon(\mathbf{r}') \mathbf{E}(\mathbf{r}') - \Delta\epsilon(\mathbf{r}) \mathbf{E}(\mathbf{r})] \\
&= -\mathbf{L}_{V_\delta} \Delta\epsilon(\mathbf{r}) \mathbf{E}(\mathbf{r}) + \int_{V_\delta} d\mathbf{r}' \nabla \nabla g_0(\mathbf{r}, \mathbf{r}') [\Delta\epsilon(\mathbf{r}') \mathbf{E}(\mathbf{r}') - \Delta\epsilon(\mathbf{r}) \mathbf{E}(\mathbf{r})], \tag{29}
\end{aligned}$$

where the second integral has a removable singularity  $O\left(\frac{1}{|\mathbf{r} - \mathbf{r}'|^2}\right)$  through the use of the spherical coordinate transform centered at  $\mathbf{r}$ , provided the function  $\Delta\epsilon(\mathbf{r}) \mathbf{E}(\mathbf{r})$  is a differentiable inside  $V_\delta$ , which we assume to be.

Using Eq. (29) and noting that  $\tilde{g} = g - g_0$  is a regular function, Eq. (25) becomes

$$\begin{aligned}
\mathbf{C} \cdot \mathbf{E} &= \mathbf{E}^{\text{inc}}(\mathbf{r}) - i\omega \mu \int_{\Omega \setminus V_\delta} i\omega \Delta\epsilon(\mathbf{r}') \bar{\mathbf{G}}_{\mathbf{E}}(\mathbf{r}, \mathbf{r}') \cdot \mathbf{E}(\mathbf{r}') \\
&\quad + \omega^2 \mu \int_{V_\delta} d\mathbf{r}' \Delta\epsilon(\mathbf{r}') \mathbf{E}(\mathbf{r}') g(\mathbf{r}, \mathbf{r}') \\
&\quad + \frac{\omega^2}{k^2} \mu \int_{V_\delta} d\mathbf{r}' \Delta\epsilon(\mathbf{r}') \nabla \nabla \tilde{g}(\mathbf{r}, \mathbf{r}') \cdot \mathbf{E}(\mathbf{r}') \\
&\quad + \frac{\omega^2}{k^2} \mu \int_{V_\delta} d\mathbf{r}' \nabla \nabla g_0(\mathbf{r}, \mathbf{r}') [\Delta\epsilon(\mathbf{r}') \mathbf{E}(\mathbf{r}') - \Delta\epsilon(\mathbf{r}) \mathbf{E}(\mathbf{r})], \tag{30}
\end{aligned}$$



with the same coefficient  $\mathbf{C}$  being defined in Eq. (20).

The VIE in (30) is similar to those obtained by Fikioris [4], however, our derivation is based on a splitting of Green's function in (26) and the identity for the  $\mathbf{L}_{V_\delta}$  in (28). A comparison study between CPV formulation (19) and finite exclusion volume formulation (30) can be found in [15]. Now expression (30) holds for any finite  $\delta > 0$  as long as  $V_\delta \subset \Omega$ , and all integration terms involved on the right hand side are well-defined provided that  $\Delta\epsilon(\mathbf{r})\mathbf{E}(\mathbf{r})$  is Hölder continuous. We can see that the last three integration terms can be understood as the correction terms for computing the Cauchy principal value with a finite-sized exclusion volume  $V_\delta$ . It should be noted that these integrals are all weakly singular integrals whose singularities can be removed by the simple spherical coordinate transform. In particular, we can easily estimate their magnitude in terms of  $\delta$ . Namely,

$$|\int_{V_\delta} d\mathbf{r}' \Delta\epsilon(\mathbf{r}') \mathbf{E}(\mathbf{r}') g(\mathbf{r}, \mathbf{r}')| \leq C_1 \|\Delta\epsilon \mathbf{E}\|_\infty \delta^2, \quad (31)$$

$$|\int_{V_\delta} d\mathbf{r}' \Delta\epsilon(\mathbf{r}') \nabla \nabla \tilde{g}(\mathbf{r}, \mathbf{r}') \cdot \mathbf{E}(\mathbf{r}')| \leq C_2 \|\Delta\epsilon \mathbf{E}\|_\infty \delta^2, \quad (32)$$

and

$$|\int_{V_\delta} d\mathbf{r}' \nabla \nabla g_0(\mathbf{r}, \mathbf{r}') [\Delta\epsilon(\mathbf{r}') \mathbf{E}(\mathbf{r}') - \Delta\epsilon(\mathbf{r}) \mathbf{E}(\mathbf{r})]| \leq C_3 \|\Delta\epsilon \mathbf{E}\|_{1,\infty} \delta, \quad (33)$$

where  $C_1, C_2, C_3$  are constants, and  $\|\cdot\|_\infty$  and  $\|\cdot\|_{1,\infty}$  represent the  $L^\infty$  norms of a function and its first derivative, respectively.

**Remark 1** Eqs. (31)-(33) explicitly indicate the accuracy of approximating the Cauchy principal value (1) by the integral (2) with a finite  $\delta > 0$ , i.e., the truncation error is of the order  $O(\delta)$ . Hence the numerical solution of the VIE will have this  $O(\delta)$  truncation error in general regardless of the integration quadratures used if terms in Eqs. (31)-(33) are not included.

However, For the case that  $V_\delta$  is a ball of radius  $\delta$  centered at  $\mathbf{r}$ , one can obtain a better estimate in Eq.(33) due to the anti-symmetry of the singular term  $\nabla \nabla g_0(\mathbf{r}, \mathbf{r}')$  in the spherical coordinates, i.e.

$$|\int_{V_\delta} d\mathbf{r}' \nabla \nabla g_0(\mathbf{r}, \mathbf{r}') [\Delta\epsilon(\mathbf{r}') \mathbf{E}(\mathbf{r}') - \Delta\epsilon(\mathbf{r}) \mathbf{E}(\mathbf{r})]| \leq C_4 \|\Delta\epsilon \mathbf{E}\|_{2,\infty} \delta^2. \quad (34)$$

### 3 Numerical Methods

#### 3.1 Nyström collocation method

Now we will use the Nyström collocation method to solve Eq. (30). First, the computational domain (scatter)  $\Omega$  is divided into  $N$  cubic elements  $\Omega_i$  with length  $a_i, i = 1, 2, \dots, N$ . On each element  $\Omega_i$ , we assign  $M$  Gauss nodes on which  $M$  scalar Lagrange basis functions  $\phi_{ij}, j = 1, 2, 3, \dots, M$  are defined and vanish outside  $\Omega_i$ . Then, we can write the solution as

$$\mathbf{E}(\mathbf{r}) = \sum_{i=1}^N \sum_{j=1}^M \mathbf{c}_{ij} \phi_{ij}(\mathbf{r}), \quad \mathbf{r} \in \Omega_i, \quad (35)$$

with  $\mathbf{c}_{ij}$  are the unknown vectorial coefficients. Inserting Eq. (35) into Eq. (30), we obtain the following equations for  $\mathbf{c}_{ij}$ :

$$\begin{aligned} \mathbf{C} \cdot \mathbf{c}_{ij} = & \mathbf{E}_{ij}^{\text{inc}} + \omega^2 \mu \sum_{n=1}^N \sum_{m=1}^M \left[ \int_{\Omega_n \setminus V_{\delta_{ij}}} d\mathbf{r}' \Delta \epsilon(\mathbf{r}') \bar{\mathbf{G}}_{\mathbf{E}}(\mathbf{r}_{ij}, \mathbf{r}') \phi_{nm}(\mathbf{r}') \right] \mathbf{c}_{nm} \\ & + \omega^2 \mu \sum_{m=1}^M \left[ \int_{V_{\delta_{ij}}} d\mathbf{r}' \Delta \epsilon(\mathbf{r}') g(\mathbf{r}_{ij}, \mathbf{r}') \phi_{im}(\mathbf{r}') \right] \mathbf{c}_{im} \\ & + \frac{\omega^2 \mu}{k^2} \sum_{m=1}^M \left[ \int_{V_{\delta_{ij}}} d\mathbf{r}' \Delta \epsilon(\mathbf{r}') \nabla \nabla \tilde{g}(\mathbf{r}_{ij}, \mathbf{r}') \phi_{im}(\mathbf{r}') \right] \cdot \mathbf{c}_{im} \\ & + \frac{\omega^2 \mu}{k^2} \sum_{m=1}^M \int_{V_{\delta_{ij}}} d\mathbf{r}' \nabla^2 g_0(\mathbf{r}_{ij}, \mathbf{r}') [\Delta \epsilon(\mathbf{r}') \phi_{im}(\mathbf{r}') - \Delta \epsilon_{ij} \phi_{im}(\mathbf{r}_{ij})] \cdot \mathbf{c}_{im}. \end{aligned} \quad (36)$$

When  $n \neq i$ , we have  $V_{\delta_{ij}} \notin \Omega$ , then in Eq. (36) the integral

$$\int_{\Omega_n \setminus V_{\delta_{ij}}} d\mathbf{r}' \Delta \epsilon(\mathbf{r}') \bar{\mathbf{G}}_{\mathbf{E}}(\mathbf{r}_{ij}, \mathbf{r}') \phi_{nm}(\mathbf{r}') \quad (37)$$

is regular on the whole cube  $\Omega_n$  and hence it can be evaluated by the regular Gauss quadratures, i.e.,

$$\int_{\Omega_n} d\mathbf{r}' \Delta \epsilon(\mathbf{r}') \bar{\mathbf{G}}_{\mathbf{E}}(\mathbf{r}_{ij}, \mathbf{r}') \phi_{nm}(\mathbf{r}') = \left( \frac{a_n}{2} \right)^3 \sum_{m=1}^M \Delta \epsilon_{nm} \bar{\mathbf{G}}_{\mathbf{E}}(\mathbf{r}_{ij}, \mathbf{r}_{nm}) \omega_m^s, \quad (38)$$

with  $\omega_m^s$  being the standard Gauss weights in 3-D, which are obtained from the tensor product of the Gauss weights in the 1-D domain  $[-1, 1]$ .

When  $n = i$ , although the singularity  $\mathbf{r}_{ij}$  is excluded from the domain  $\Omega_i$ ,

the calculation of the integral

$$\int_{\Omega_i \setminus V_{\delta_{ij}}} d\mathbf{r}' \Delta\epsilon(\mathbf{r}') \bar{\mathbf{G}}_{\mathbf{E}}(\mathbf{r}_{ij}, \mathbf{r}') \phi_{im}(\mathbf{r}') \quad (39)$$

is still challenging. Next, we present an efficient quadrature formula to evaluate this integral.

### 3.2 Interpolated weights on Gauss nodes for integrals on $\Omega \setminus V_\delta$

For the sake of generality, we consider the following integral:

$$I_s = \int_{\Omega \setminus V_\delta} \frac{f(\mathbf{r}; \mathbf{r}') h(\mathbf{r}; \mathbf{r}')}{R^k} d\mathbf{r}', \quad \mathbf{r} \in V_\delta, \quad (40)$$

where  $k = 1, 2, 3$  corresponds to weak, strong, and hyper-singularity of the integral, respectively. The function  $f(\mathbf{r}; \mathbf{r}')$  is assumed to be a general smooth and well-defined function, while  $h(\mathbf{r}; \mathbf{r}')$  is a fixed arbitrary function which results from the directional derivative in the definition of the dyadic Green's functions.

As the function  $f(\mathbf{r}; \mathbf{r}')$  is smooth over the whole domain  $\Omega$ , then it can be well approximated by the following simple interpolation:

$$f(\mathbf{r}; \mathbf{r}') \approx \sum_{j=1}^J f(\mathbf{r}; \mathbf{r}_j) \phi_j(\mathbf{r}'), \quad \mathbf{r}_j \in \Omega, \quad (41)$$

where  $\{\mathbf{r}_j\}_{j=1}^J$  are  $J$ -nodes in  $\Omega$  formed by the tensor product of Gauss node in  $[-1, 1]$ . Combining Eqs. (40) and (41) yields

$$\int_{\Omega \setminus V_\delta} \frac{f(\mathbf{r}; \mathbf{r}') h(\mathbf{r}; \mathbf{r}')}{R^k} d\mathbf{r}' \approx \sum_{j=1}^J f(\mathbf{r}; \mathbf{r}_j) \omega_j^e, \quad (42)$$

We call  $\omega_j^e$  the effective interpolated weights, or just *interpolated weights*, which are defined through the integral

$$\omega_j^e = \int_{\Omega \setminus V_\delta} \frac{\phi_j(\mathbf{r}') h(\mathbf{r}; \mathbf{r}')}{|\mathbf{r} - \mathbf{r}'|^k} d\mathbf{r}'. \quad (43)$$

Note that the interpolated weights  $\omega_j^e$  depend on the location of the singularity  $\mathbf{r}$  and relies on accurate calculations of Eq. (43), which will be accomplished in two steps: first the domain  $\Omega$  is subdivided into nine cubes with one containing the singularity  $\mathbf{r}$  in its center. For the cube including the singularity, a straight-forward, brute-force approach involving a large number  $N$  ( $N \gg J$ ) of Gauss points is adopted in local spherical polar coordinates, will be used to obtain

satisfactory accuracy. While for the other cubes, regular tensor product Gauss quadrature is applied. Details of the computations and resulting weight tables could be found in [17].

Fortunately, the computation of weights  $\omega_j^\varepsilon$  only needs to be performed once and tabulated for the reference domain, then they can be used for various cubic elements. Due to the smoothness of function  $f(\mathbf{r}, \mathbf{r}')$ , the number  $J$  is relatively small, especially if the element size is small as in practice, so computation of Eq. (39) is now efficient once  $\omega_j^\varepsilon$  are obtained.

**Remark 2** *As the Cauchy principal value in the VIE, thus the VIE itself, depends on the specific shape of the exclusion volume, the interpolated weights can only be used for the shape for which it was calculated, namely, a cubic shape here. So, for a general element obtained by an affine mapping as in a finite element triangulation, we will need to isolate the singularity by a cube with the singularity at its center, then the pre-calculated interpolated weights defined in (43) can be used while integral over the rest of the region outside the cube within the element of a more general shape can be done with regular Gauss quadratures.*

### 3.3 Computation of VIE matrix entries

In this section, we will show how to compute the matrix entries accurately for the VIE in the following steps.

- Step I: calculate interpolated weights on the reference cubic domain.

For Eq. (43), we take  $\Omega = [-1, 1]^3$  and  $V_\delta = B(\mathbf{r}_j, \delta)$ , where  $\delta > 0$  is a prescribed small number and  $\mathbf{r}_j, j = 1, 2, \dots, M$  coincident with the coordinates of  $M$  Gauss points in the reference domain, and we take  $J = M$  in Eq. (41).

Further, the dyadic Green's function has the form

$$\begin{aligned} \overline{\mathbf{G}}_{\mathbf{E}} = g\mathbf{I} + \frac{\nabla^2 g}{k^2} &= \frac{e^{-ikR}}{4\pi R}(\mathbf{I} - \mathbf{u} \otimes \mathbf{u}) \\ &- \frac{ie^{-ikR}}{4\pi R^2 k}(\mathbf{I} - 3\mathbf{u} \otimes \mathbf{u}) - \frac{e^{-ikR}}{4\pi R^3 k^2}(\mathbf{I} - 3\mathbf{u} \otimes \mathbf{u}). \end{aligned} \quad (44)$$

Since the value of function  $\mathbf{u} \otimes \mathbf{u}$  is multiple-defined at  $R = 0$ , in (40) we need to take

$$h(\mathbf{r}; \mathbf{r}') = \mathbf{u} \otimes \mathbf{u}, \quad (45)$$

and hence Eq. (43) yields a set of 9 interpolated weight matrices. However, due to the symmetry of the matrix  $\mathbf{u} \otimes \mathbf{u}$ , only 6 components need to be

calculated. For the identity matrix  $\mathbf{I}$  term in Eq. (44), we will also need a set of scalar interpolation weights by assuming  $h(\mathbf{r}, \mathbf{r}') = 1$  in (43).

Additionally, for the scalar and matrix weights, we need to calculate for  $k = 1, 2$ , and 3 for weak, strong, and hyper singular integrals, respectively.

To summarize, for each collocation point (also the singularity location)  $\mathbf{r}_j, j = 1, 2, \dots, M$  in an element, scalar weights  $\omega_{j,m}, \bar{\omega}_{j,m}$  and  $\tilde{\omega}_{j,m}, m = 1, 2, \dots, M$  are calculated for weak, strong, hyper-singular integrals, respectively. And the corresponding weights are denoted as  $\Lambda_{j,m}, \bar{\Lambda}_{j,m}$ , and  $\tilde{\Lambda}_{j,m}$ . These weights only need to be calculated once and then stored for future use.

- Step II: We discretize the computational domain into a series of cubic elements with length  $a_i, i = 1, 2, \dots, N$  and assign  $M$  Gauss points in each elements. For the  $j$ -th Gauss point  $\mathbf{r}_{ij}$  in the  $i$ -th element, we construct the equation:

$$-\omega^2 \mu \sum_{n=1}^N \sum_{m=1}^M \mathbf{A}_{nm} \cdot \mathbf{c}_{nm} - \sum_{m=1}^M \mathbf{B}_{im} \cdot \mathbf{c}_{im} + \left(1 + \frac{1}{3} \Delta \epsilon_{ij}\right) \mathbf{I}_{3 \times 3} \cdot \mathbf{c}_{ij} = \mathbf{E}_{ij}^{\text{inc}}, \quad (46)$$

The matrix  $\mathbf{B}$  originates from the correction terms of the Cauchy principal value

$$\begin{aligned} \mathbf{B}_{im} &= \omega^2 \mu \int_{B(\mathbf{r}_{ij}, a_i \delta)} d\mathbf{r}' \Delta \epsilon(\mathbf{r}') g(\mathbf{r}_{ij}, \mathbf{r}') \phi_{im}(\mathbf{r}') \\ &+ \frac{\omega^2 \mu}{k^2} \int_{B(\mathbf{r}_{ij}, a_i \delta)} d\mathbf{r}' \Delta \epsilon(\mathbf{r}') \nabla^2 \tilde{g}(\mathbf{r}_{ij}, \mathbf{r}') \phi_{im}(\mathbf{r}') \\ &+ \frac{\omega^2 \mu}{k^2} \int_{B(\mathbf{r}_{ij}, a_i \delta)} d\mathbf{r}' \nabla^2 g_0(\mathbf{r}_{ij}, \mathbf{r}') [\Delta \epsilon(\mathbf{r}') \phi_{im}(\mathbf{r}') - \Delta \epsilon_{ij} \phi_{im}(\mathbf{r}_{ij})], \quad (47) \end{aligned}$$

and it can be calculated by standard Gauss quadrature through spherical coordinates since the Jacobian will eliminate completely the singularity of the integrands.

When  $n = i$ , we calculate the integral Eq.(39) as

$$\begin{aligned} \mathbf{A}_{im} &= \frac{1}{4\pi} \left(\frac{a_i}{2}\right)^3 \sum_{j=1}^M \Delta \epsilon_{im} \left[ \left( e^{-ikR_m} \omega_{j,m}^i - ie^{-ikR_m} \bar{\omega}_{j,m}^i - e^{-ikR_m} \tilde{\omega}_{j,m}^i \right) \mathbf{I}_{3 \times 3} \right. \\ &\quad \left. e^{-ikR_m} \Lambda_{j,m}^i - ie^{-ikR_m} \bar{\Lambda}_{j,m}^i - e^{-ikR_m} \tilde{\Lambda}_{j,m}^i \right], \quad (48) \end{aligned}$$

where  $R_m = |\mathbf{r}_{ij} - \mathbf{r}_{im}|$  and recall the definition of the interpolated weights Eq. (43), we have

$$\begin{aligned} \omega_{j,m}^i &= \left(\frac{2}{a_i}\right) \omega_{j,m}, \quad \bar{\omega}_{j,m}^i = \left(\frac{2}{a_i}\right)^2 \bar{\omega}_{j,m}, \quad \tilde{\omega}_{j,m}^i = \left(\frac{2}{a_i}\right)^3 \tilde{\omega}_{j,m}, \\ \Lambda_{j,m}^i &= \left(\frac{2}{a_i}\right) \Lambda_{j,m}, \quad \bar{\Lambda}_{j,m}^i = \left(\frac{2}{a_i}\right)^2 \bar{\Lambda}_{j,m}, \quad \tilde{\Lambda}_{j,m}^i = \left(\frac{2}{a_i}\right)^3 \tilde{\Lambda}_{j,m}, \quad (49) \end{aligned}$$

when  $n \neq i$ , we have

$$\mathbf{A}_{nm} = \left(\frac{a_n}{2}\right)^3 \sum_{j=1}^M \Delta\epsilon_{nm} \bar{\mathbf{G}}_{\mathbf{E}}(\mathbf{r}_{ij}, \mathbf{r}_{nm}) \omega_j^s. \quad (50)$$

- Step III: Eq. (46) for all the  $N \times M$  Gauss points can be assembled as the following linear algebraic equation system

$$\mathbf{V} \cdot \vec{\mathbf{c}} = \begin{bmatrix} \mathbf{V}_{xx} & \mathbf{V}_{xy} & \mathbf{V}_{xz} \\ \mathbf{V}_{yx} & \mathbf{V}_{yy} & \mathbf{V}_{yz} \\ \mathbf{V}_{zx} & \mathbf{V}_{zy} & \mathbf{V}_{zz} \end{bmatrix} \cdot \begin{bmatrix} \mathbf{c}_x \\ \mathbf{c}_y \\ \mathbf{c}_z \end{bmatrix} = \begin{bmatrix} \mathbf{E}_x^{\text{inc}} \\ \mathbf{E}_y^{\text{inc}} \\ \mathbf{E}_z^{\text{inc}} \end{bmatrix}. \quad (51)$$

Based on the properties of the Green's function, the  $3NM \times 3NM$  matrix  $\mathbf{V}$  is partitioned into nine blocks, each of which is a  $NM \times NM$  sub-matrix. The solution of the VIE contains three  $NM \times 1$  vectors, which represents the field in  $x$ ,  $y$ , and  $z$  directions. This system is solved by iteration methods such as the GMRES method.

## 4 Numerical Results

In this section we test the accuracy of the interpolated weights on Gauss nodes, the  $\delta$ -independence of the solution of the VIE, and convergence of the  $p$ -refinement of the Nyström collocation method.

### 4.1 Accuracy of the interpolated weights on Gauss nodes

In Eq. (46), the calculation of matrix  $\mathbf{B}$  from the correction terms are straightforward, so we will focus on validating the interpolated weights in computing matrix  $\mathbf{A}$ . For convenience, we consider the integral of a real-valued, tensor function

$$\frac{\cos R}{R}(\mathbf{I} - \mathbf{u} \otimes \mathbf{u}) + \frac{\cos R}{R^2}(\mathbf{I} - 3\mathbf{u} \otimes \mathbf{u}) + \frac{\cos R}{R^3}(\mathbf{I} - 3\mathbf{u} \otimes \mathbf{u}), \quad (52)$$

which is similar to the Green's function Eq. (44) on the domain  $\Omega \setminus V_\delta$ . Without loss of generality, we take  $\Omega = [-1, 1]^3$  and  $\mathbf{r}_j$  as the 27 points constructed from the tensor product of the Gauss points of order 3 in  $[-1, 1]$ . Thus, we have  $j = m = 1, 2, \dots, 27$  as in Eq.(49) and the integral yields

$$\mathbf{G}_j \approx \sum_{m=1}^{27} \cos(|\mathbf{r}_m - \mathbf{r}_j|) \left[ (\omega_{j,m} + \bar{\omega}_{j,m} + \tilde{\omega}_{j,m}) \bar{\mathbf{I}} - \Lambda_{j,m} - 3\bar{\Lambda}_{j,m} - 3\tilde{\Lambda}_{j,m} \right], \quad (53)$$

Table 1

Convergence of the integral as the singularity is at center.  $g_{11} = g_{22} = g_{33}$  and  $g_{12} = g_{13} = g_{23} = 0$ .

	$\delta = 0.1$	$\delta = 0.05$	$\delta = 0.025$	$\delta = 0.0125$
$g_{11}$	3.985701	4.017024	4.024872	4.026835
error	-4.1784E-2	-1.0461E-2	-2.613E-3	-6.5E-4
order	-	2	2	2

Table 2

Convergence of the integral as singularity is at a corner. Reference solution  $g_{11} = g_{22} = g_{33} = 0.982526$  and  $g_{12} = g_{13} = g_{23} = -0.998097$ .

	$\delta = 0.1$	$\delta = 0.05$	$\delta = 0.025$	$\delta = 0.0125$
$g_{11}$	0.940714	0.972063	0.979913	0.981876
error	-2.80425E-1	-7.3424E-2	-1.8102E-2	-3.983E-3
order	-	1.93	2	2.1
$g_{12}$	-0.998084	-0.998094	-0.998097	-0.998097
error	1.3E-5	3.0E-6	0	0
order	-	2.1	-	-

which is a  $3 \times 3$  matrix depending on  $\mathbf{r}_j$ .

For each  $\mathbf{G}_j$ , we use the direct brute force method introduced in [17] to obtain the reference solution with the very small  $\delta = 10^{-3}$ . Then we calculate the integral using the interpolated weights as in Eq.(53) with different values of  $\delta$ . According to the previous analysis, the differences with the reference solution should decay in the order  $O(\delta^2)$  as  $\delta$  decreases, which will be checked in the following.

We classify the 27 sets of weights into four categories, based on the position of the singularity  $\mathbf{r}_j$ , as the ones near the corner, edge, face, and center of the cube. The matrix  $\mathbf{G}_j$  is symmetric, so we only check the three diagonal entries ( $g_{11}$ ,  $g_{22}$ , and  $g_{33}$ ) and the three upper diagonal entries ( $g_{12}$ ,  $g_{13}$ , and  $g_{23}$ ).

Table 1 presents the numerical results when the singularity  $\mathbf{r}_j$  is located in the center of the cube, in which case  $g_{11} = g_{22} = g_{33}$  and the off-diagonal entries are all zeros. The values of  $\delta$  are taken as 0.1, 0.05, 0.025, and 0.0125 while the reference solution is  $g_{11} = 4.027477$ .

In a similar fashion, Tables 2-4 show the accuracies when the singularity is located near the corner, edge, and face of the cube, respectively. Comparing to the reference solutions, the expected second-order decay with respect to the

Table 3

Convergence of the integral as singularity is at an edge. Reference solutions  $g_{11} = -1.515302$ ,  $g_{22} = g_{33} = 3.39234$ ,  $g_{23} = -1.579086$  and  $g_{12} = g_{13} = 0$ .

	$\delta = 0.1$	$\delta = 0.05$	$\delta = 0.025$	$\delta = 0.0125$
$g_{11}$	-1.559532	-1.526351	-1.518059	-1.515987
error	-4.423E-2	1.1049E-2	2.757E-3	-6.85E-4
order	-	2	2	2
$g_{22}$	3.35175	3.38217	3.389798	3.391707
error	-4.059E-2	-1.1017E-2	2.542E-3	-6.33E-4
order	-	1.9	2.1	2
$g_{23}$	-1.579072	-1.579082	-1.579085	-1.579085
error	1.4E-5	4.0E-6	1.0E-6	1.0E-6
order	-	1.8	2	0

Table 4

Convergence of the integral as singularity is at a face. Reference solutions  $g_{11} = 0.877428$ ,  $g_{22} = 0$ ,  $g_{33} = 6.494784$ , and  $g_{12} = g_{13} = g_{23} = 0$ .

	$\delta = 0.1$	$\delta = 0.05$	$\delta = 0.025$	$\delta = 0.0125$
$g_{11}$	0.83442	0.866672	0.874742	0.87676
error	-4.3008E-2	-1.10756E-2	-2.686E-3	-6.68E-4
order	-	1.9	2	2
$g_{33}$	6.455419	6.484909	6.492315	6.49417
error	-3.9365E-2	-9.875E-3	-2.469E-3	-6.14E-4
order	-	2	2	2

$\delta$  is confirmed.

#### 4.2 $\delta$ -independence of the VIE solution

Equation (30) provides a formulation from which the solution of the VIE will be independent of the choice of a specific  $\delta$ . In the following tests, we take  $\mu = 1$ ,  $\Delta\epsilon = 4$ ,  $\omega = 1$  and solve the VIE. The computation domain is taken as  $[-\pi/2, \pi/2]^3$ , while the incident wave is

$$\mathbf{E}_x^{\text{inc}} = e^{ik(-y+0.5z)}, \quad \mathbf{E}_y^{\text{inc}} = \mathbf{E}_z^{\text{inc}} = 0.$$



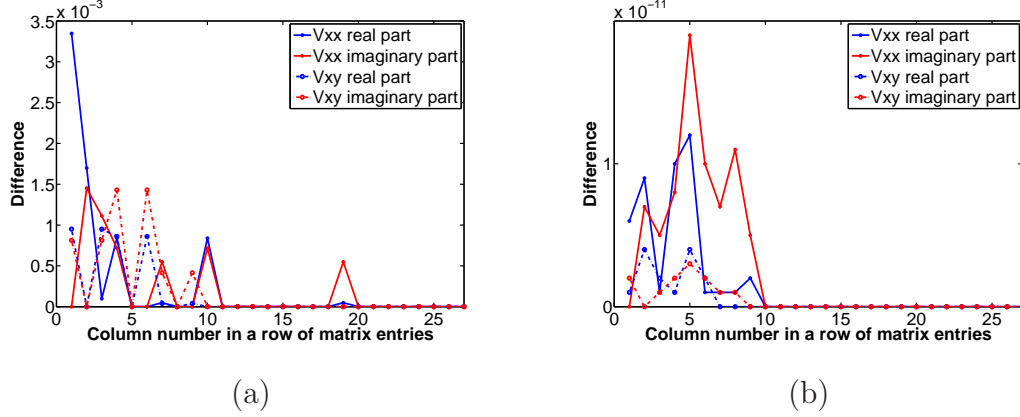


Fig. 1. Differences of matrix entries with  $\delta=0.1$  and  $\delta = 0.001$ . (a): without correction terms; (b) with correction terms.

We first check the  $\delta$ -independence of the matrix entries in Eq. (51). Figure 1 displays the differences of one row of entries in the matrix  $\mathbf{V}$  between the choices of  $\delta = 0.1$  and  $\delta = 0.001$ , in which the solid lines are for the entries from a diagonal block ( $V_{xx}$ ) and dashed lines are for the entries from an off-diagonal block ( $V_{xy}$ ). The blue curves are for real while red curves are for imaginary parts. From Fig. 1(a) we can see that the differences between entries in the corresponding positions can be as large as  $3.0 \times 10^{-3}$  when the correction terms are not included. In contrast, the corresponding differences are reduced to below  $2 \times 10^{-11}$  when the corrections are, hence the matrix entries are  $\delta$ -independent.

Next we check the  $\delta$ -dependence of the overall solution of the VIE. The solution of VIE with a very small  $\delta = 0.001$  is taken as the reference solution. Then various choices of  $\delta$  are taken and the differences of the corresponding solutions with the reference solution are calculated. The differences are measured in the  $L^\infty$  norm for the three components  $E_x$ ,  $E_y$ ,  $E_z$  and they are listed in Tables 5-6.

Table 5

Comparison of solutions of the VIE without the correction terms

	$\delta = 0.1$	$\delta = 0.05$	$\delta = 0.025$	$\delta = 0.0125$
$\ E_x - E_x^{\text{ref}}\ _{L^\infty}$	3.360E-3	8.264E-4	2.044E-4	5.039E-5
$\ E_y - E_y^{\text{ref}}\ _{L^\infty}$	1.476E-3	3.696E-4	9.258E-5	2.358E-5
$\ E_z - E_z^{\text{ref}}\ _{L^\infty}$	2.533E-3	6.387E-4	1.597E-4	3.969E-5

From Table 5 it can be seen that without the correction terms, the solution of VIE has an obvious dependence on the choice of  $\delta$  and the differences follow the order of  $O(\delta^2)$ , while the solution is indeed  $\delta$ -independent when the correction terms are included, as shown in Table 6.

Table 6

Comparison of solutions of the VIE with the correction terms

	$\delta = 0.1$	$\delta = 0.05$	$\delta = 0.025$	$\delta = 0.0125$
$\ E_x - E_x^{\text{ref}}\ _{L^\infty}$	8.0E-12	1.0E-12	0	0
$\ E_y - E_y^{\text{ref}}\ _{L^\infty}$	2.0E-12	1.0E-12	0	0
$\ E_z - E_z^{\text{ref}}\ _{L^\infty}$	1.0E-12	0	0	0

#### 4.3 $p$ -convergence of the VIE

For numerical convergence, one can discretize the computational domain into finer elements (increasing the number  $N$ ,  $h$ -refinement) or use higher order polynomial basis (increasing the number  $M$ ,  $p$ -refinement) for the integral in the VIE. In the current work we focus on the latter since the emphasis is on the accurate calculation of the Cauchy principal value of the integral with singularities in the domain.

In the following tests, the Lagrange interpolation of the solution of the VIE with  $M = 7$  (namely, 6th order polynomial basis functions) is taken as the reference solution  $\mathbf{E}^{\text{ref}}$  and differences between the solutions  $\mathbf{E}^M$ ,  $M = 3, 4, 5, 6$  are taken. We consider the linear relation between the  $\log_{10}$  of the energy error

$$\text{Error} = \|\mathbf{E}^M - \mathbf{E}^{\text{ref}}\|_{L^2(\Omega)},$$

and the order  $p = M - 1$  of polynomial basis function, i.e.

$$\log_{10}(\text{Error}) = kp + b,$$

where  $k$  and  $b$  are parameters. In Fig. 2 there plots the  $\log_{10}$  error against the order  $p$ , as well as the fitted lines, for the solution components  $E_x$ ,  $E_y$ , and  $E_z$  respectively. It can be seen that the  $\log_{10}(\text{Error})$  decays linearly with respect to  $p$ . Quantitatively, we obtain

$$\begin{aligned} k &= -0.464, & b &= -0.092, & \text{for } E_x \\ k &= -0.353, & b &= -0.763, & \text{for } E_y. \\ k &= -0.391, & b &= -0.946, & \text{for } E_z. \end{aligned}$$

Hence we conclude that the exponential convergence is achieved for the errors against the order  $p$ .

Figure 3 is a 3D plot of the incident wave and resulting electric fields inside the cubic scatter. Rows 1-3 of Fig. 3 are for the computations with Gauss node  $M = 3, 5, 7$ , respectively, and from the left to the right are the electric field components  $E_x$ ,  $E_y$ ,  $E_z$  and the incident wave  $\mathbf{E}_x^{\text{inc}}$ , respectively.

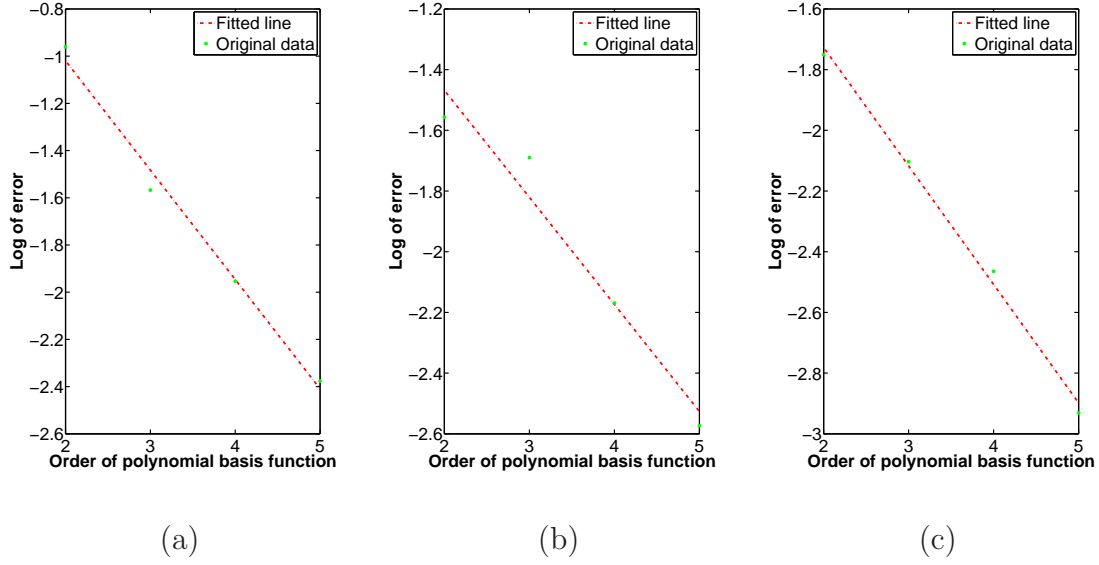


Fig. 2.  $\log_{10}$  errors of solutions against order of polynomial basis functions for  $E_x$  (a),  $E_y$  (b), and  $E_z$  (c).

Figure 4 displays the electric field in the free space where nine cubic scatterers are embedded. In order to clearly illustrate the wave interactions among the scatter array, only the scattering field  $\mathbf{E}(\mathbf{r}) - \mathbf{E}^{\text{inc}}(\mathbf{r})$  are shown in contours in a specific cross-section plane. In these tests, the incident wave is taken as

$$\mathbf{E}_x^{\text{inc}} = \mathbf{E}_y^{\text{inc}} = 0, \quad \mathbf{E}_z^{\text{inc}} = e^{ik(-2x+2y)}.$$

Each cube has a length of 0.5 and they form a  $3 \times 3$  array align in the  $x$ - $y$  plane. The coordinate of the center of the first cube is  $(0.25, 0.25, 0.25)$ . We consider two cases: in the first case the cubes are relatively far way from each other (0.25 apart) and in the second case the cubes are relatively closer (0.1 apart). In each case a lower permittivity ( $\Delta\epsilon = 4$ ) and a higher permittivity ( $\Delta\epsilon = 16$ ) are taken. Contours of the electric field  $E_x$  in the plane  $z = -0.1$  are shown in Fig 4. The first and second rows are for the scatters with smaller and bigger distances, respectively, in which the left is for  $\Delta\epsilon = 4$  and the right is for  $\Delta\epsilon = 16$ . It can be seen that the electric waves have stronger interactions when scatters are closer to each other.

## 5 Conclusion

In this paper, we have developed an highly accurate and efficient method to solve numerically the volume integral equation (VIE) of the Maxwell equation involving the Cauchy principal value of the singular dyadic Green's function.

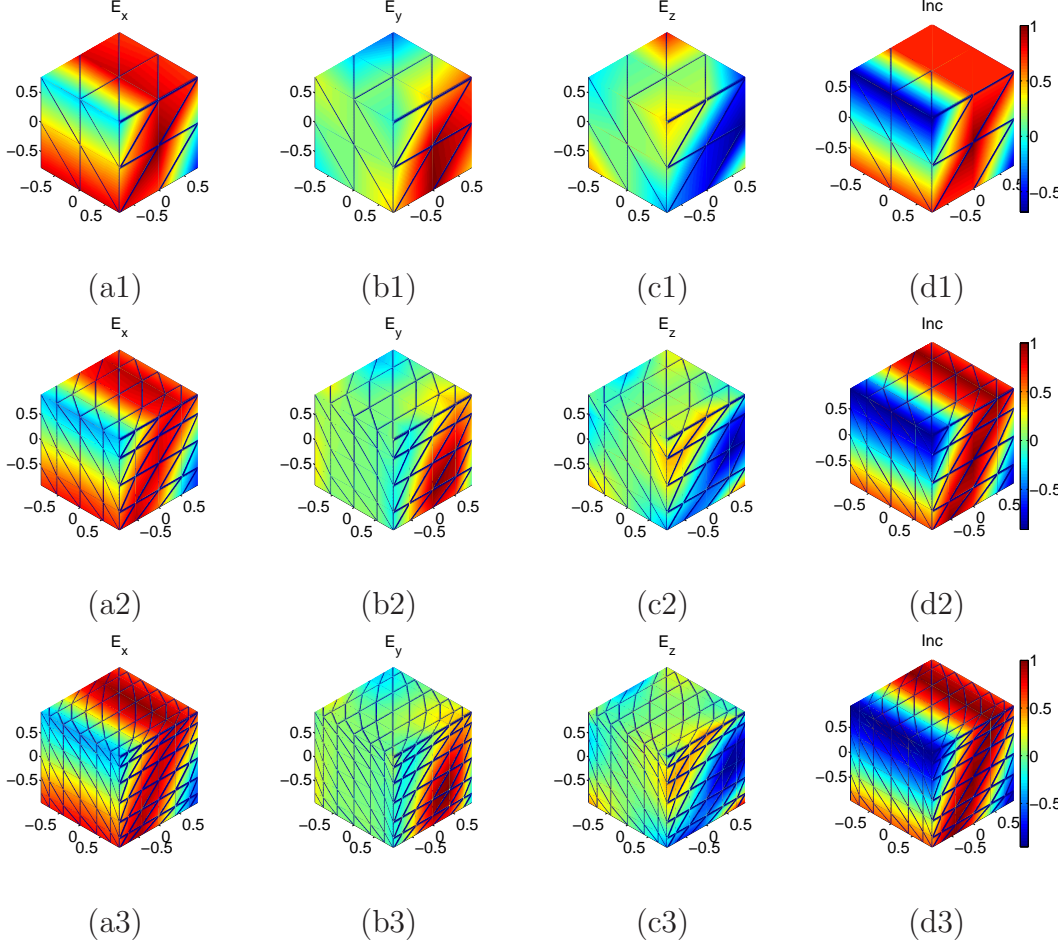


Fig. 3. Electric field and the incident wave with  $M = 3$  (first row),  $M = 5$  (second row), and  $M = 7$  (third row).

The VIE used allows us to compute the CPV for finite size exclusion volume  $V_\delta$  without truncation errors (of the order of  $O(\delta)$  in general and it is  $O(\delta^2)$  when the excluded volume is a sphere), which were accurately accounted for by including correction terms. With the correction terms, the numerical solution of the VIE will be  $\delta$ -independent. In addition, an efficient quadrature formula has been introduced to accurately compute the  $\frac{1}{R^3}$  type integration on the domain  $\Omega \setminus V_\delta$ . Finally, a Nyström collocation method based on the proposed quadrature formula were applied to the VIE resulting in an accurate and  $\delta$ -independent solution of the electric field.

The developed algorithms are verified with several numerical tests. First, the accuracy of the interpolated quadrature weights for dyadic Green's function was confirmed for various locations of the spherical exclusion volume  $V_\delta$  inside a cubic scatter. Secondly, the procedure of computing the Cauchy principal values for the dyadic Green's function with a finite size  $\delta$  is shown to be accurate with the help of the proposed correction terms. As a result, the so-

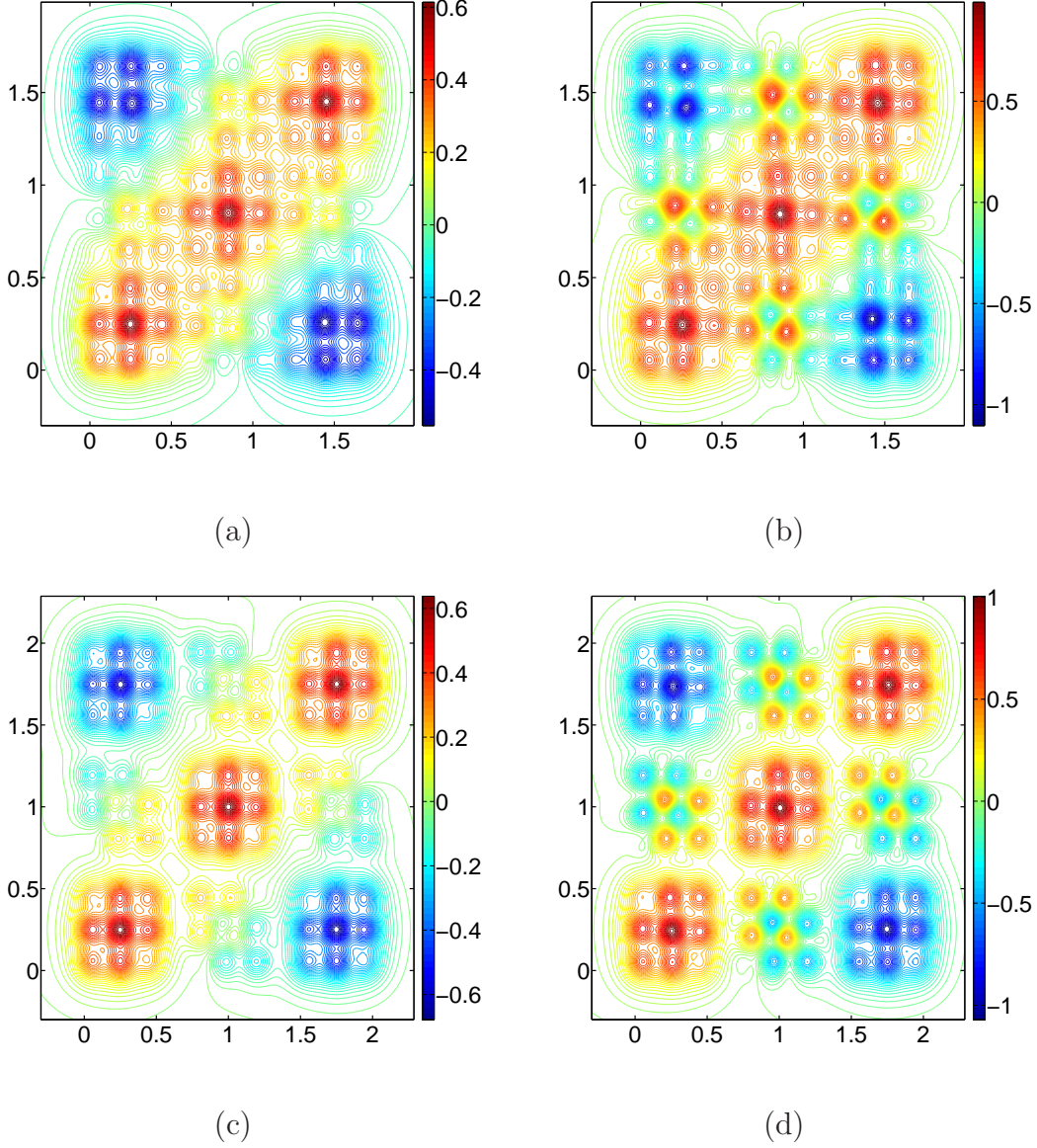


Fig. 4. Contours of the electric field from scatter arrays. (a)-(b): scatterers are 0.1 apart from each other; (c)-(d): scatterers are 0.25 apart from each other. (a, c):  $\Delta\epsilon = 4$ ; (b, d):  $\Delta\epsilon = 16$ .

lution of the VIE is shown to be  $\delta$ -independent, and finally, we demonstrated the convergence of the VIE for  $p$ -refinement with increasing order of basis functions  $p = m - 1$ , where the number of Gauss node along each direction  $m = 3, 4, 5, 6$ , and 7, respectively.

## References

- [1] Harry Atwater. The promise of Plasmonics. *Scientific American*, pages 56–62, 2007.
- [2] Harry Atwater and A. Polman. Plasmonics for improved photovoltaic devices. *Nature materials*, pages 205–213, 2010.
- [3] Wei Cai. *Computational Methods for Electromagnetic Phenomena: electrostatics in solvation, scattering, and electron transport*. Cambridge University Press, 2013.
- [4] Fikioris. Electromagnetic Field inside a Current-Carrying Region. *Journal of Mathematical Physics*, pages 1617–1620, 1965.
- [5] Y.Q. Fu and X. Zhou. Plasmonic lenses: a review. *Plasmonics*, pages 287–310, 2010.
- [6] K. Hering, D. Cialla, K. Ackermann, T. Dörfel, R. Möller, H. Schneidewind, R. Mattheis, W. Fritzsche, P. Rösch, and J. Popp. Plasmonic lenses: a review. *SERS: a versatile tool in chemical and biochemical diagnostics*, pages 113–124, 2008.
- [7] J.P. Kottmann and J.F. Martin, O. Accurate solution of the Volume Integral Equation for high-permittivity scatters. . *IEEE Transaction on Antennas and Propagation*, pages 1719–1726, 2000.
- [8] S.W. Lee, J. Boersma, C.L. Law, and G.A. Deschamps. Singularity in Green’s function and its numerical evaluation. *IEEE Transaction on Antennas and Propagation*, pages 311–317, 1980.
- [9] G Liu and S.D. Gedney. High-order Nyström solution of the Volume-EFIE for TE-wave scattering. *Electromagnetics*, pages 1–14, 2001.
- [10] J.B. Pendry. Negative refraction makes a perfect lens. *Physical Review Letters*, pages 3966–3969, 2000.
- [11] Heinz Raether. *Surface plasmons on smooth and rough surfaces and gratings*. Springer Tracts in Modern Physics, 1988.
- [12] C.V. Raman and K.S. Krishnan. A new type of secondary radiation. *Nature*, page 501, 1928.
- [13] J.A Stratton. *Electromagnetic Theory*. New York: McGraw-Hill, 1941.
- [14] M.S. Tong, Z.G. Qian, and W.C. Chew. Nyström Method Solution of Volume Integral Equations for Electromagnetic Scattering by 3D Penetrable Objects. *IEEE Transaction on Antennas and Propagation*, pages 1645–1652, 2010.
- [15] J.J.H. Wang. A Unified and Consistent View on the Singularities of the Electric Dyadic Green’s Function in the Source Region. *IEEE Transaction on Antennas and Propagation*, pages 463–468, 1982.

- [16] A.D. Yaghjian. Electric Dyadic Green's functions in the source region. *Proceedings of the IEEE*, pages 248–263, 1980.
- [17] Brian Zinser, Duan Chen, and Wei Cai. Quadrature Weights on Gauss Nodes for Accurate Integration of Singular Functions over a Cube. *preprint*, 2015.